Research on Wavelength Demodulation Algorithm for Fiber Bragg Grating Weak Signal Based on Hilbert Transform

Tao Li, Chuan Dong, Ying Geng, Tianmin Zhang, Jiejun Lin, Weijie Jiang, and Yinguo Huang

Abstract In order to improve the demodulation accuracy of the tunable F-P filter, the Hilbert transform is introduced into the Gauss fit algorithm to solve the problem of sidelobe or peak distortion in the low power and low signal-to-noise ratio. First, digital low-pass filtering is used to complete the data pre-processing, then using the peak-seek algorithm designed in this paper to confirm the peak position of the two signals, and finally using the linear interpolation algorithm to demodulate the FBG center wavelength. Demodulation experiments show that the demodulation method used in this paper has the advantages of small computation, high demodulation accuracy and less than 1 pm peak seeking error.

Keywords Fiber Bragg grating · Wavelength demodulation · Tunable F-P filter · Hilbert transform · Gauss fit algorithm

1 Introduction

Fiber Bragg Grating (FBG), as a wavelength modulated sensor, reflects the changes of measured physical quantities by wavelength modulation of the sensing signal [1]. Its central wavelength can be used to measure parameters such as strain [2], temperature [3], pressure [4], humidity [5], vibration [6], viscosity [7], etc. But in practical applications, the FBG center wavelength is obtained by the corresponding peak-seek method, so the detection accuracy of FBG sensor networks is closely related to the peak-seek accuracy of its demodulation algorithm.

Commonly used peak-seek algorithms include direct peak-seek algorithm, power weighted peak-seek algorithm, general polynomial fitting, and Gaussian fitting algorithm, etc. Among which Gaussian fitting algorithm has the advantages of good noise

T. Li · J. Lin · W. Jiang
Shanghai Marine Equipment Research Institute, Shanghai, China

C. Dong · Y. Geng · T. Zhang · Y. Huang (✉)
Tianjin University, Tianjin, China
e-mail: hyg@tju.edu.cn

immunity and small error, and the related improved algorithm is also the most. Hu et al. [7] optimized the fitting coefficients of Gauss curve by LM algorithm, which reduced the peak-seek error of FBG demodulation algorithm effectively; Jiang et al. [8] proposed a Weighted Least Squares fitting combined with Asymmetric Gauss correction (WLS-AG) algorithm to achieve high precision peak-seek for the sampled ultra weak fiber Bragg gratings with interference noise; Zhai and Li [9] designed a Gauss curve fitting method (WTG) based on the Wavelets Transform to improve the demodulation accuracy at low sampling rates. Djurhuus et al. [10] proposed a signal processing method for FBG temperature measurements based on the machine learning tool Gauss Process Regression (GPR). Experiments show that the method has lower error and higher detection accuracy.

However, when the FBG reflected light signal has low power, low signal-to-noise ratio, and multiple peaks, traditional demodulation algorithms suffer from low accuracy, poor noise resistance, and false peak detection. This paper combines Hilbert transform with Gauss fitting algorithm to achieve multi peak detection, while reducing the amount of demodulation algorithm operations and improving the demodulation accuracy.

2 Principles of Tunable F-P Filter Demodulation System

The tunable F-P filter demodulation method has the advantages of high accuracy, wide demodulation range, and the ability to achieve multiplexing of large-scale FBG sensor networks. The principle of tunable F-P filter demodulation technology based on F-P etalon is shown in Fig. 1, where the function of F-P etalon is to perform nonlinear calibration on tunable F-P filter.

A broad-band optical signal from ASE broadband light source enters Tunable F-P Filter, which is controlled by Drive circuit to transmit narrow-band optical signals
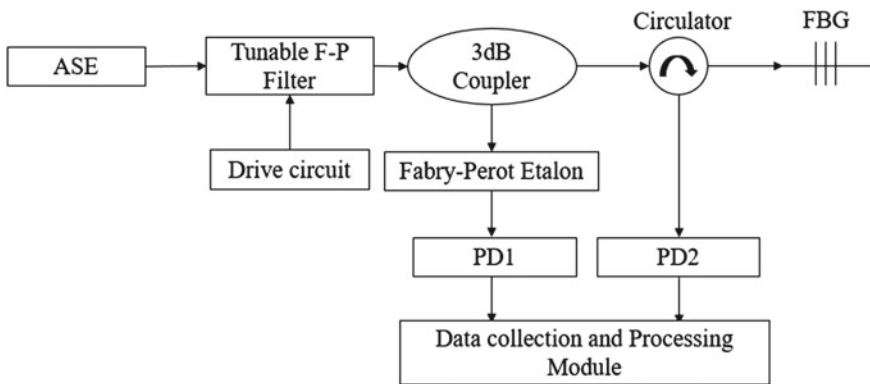

Fig. 1 Schematic diagram of tunable F-P filter demodulation principle based on F-P etalon

with different central wavelengths. The narrow-band optical signal enters the F-P Etalon one way through a 3 dB Coupler, its transmitted signal is detected by PD1, the other way through Circulator into the FBG, and the reflected optical signal is detected by PD2 when the narrow-band light transmitted by the Tunable F-P Filter meets the FBG Bragg condition. After the Data collection and Processing module, the peak-seek algorithm, curve fitting and other data processing are completed in the computer, thus wavelength demodulation of FBG is achieved.

3   Research on FBG Demodulation Algorithms

The overall flow of the center wavelength demodulation algorithm in this article is shown in Fig. 2.

First read the two signals from the FBG and F-P Etalon, the second is digital low-pass filtering is performed to complete data pre-processing, the next is to confirm the peak position of the two signals using the peak-seek algorithm designed in this paper, finally, the FBG center wavelength is demodulated using a linear interpolation algorithm.

3.1   Digital Low-Pass Filter Processing

First, digital low-pass filtering is performed on the acquired raw data to filter out part of the high-frequency noise introduced during the acquisition. Digital filters are divided into Finite Impulse Response Filter (FIR) and Infinite Impulse Response Filter (IIR), the differences between which are shown in Table 1. In order to reduce
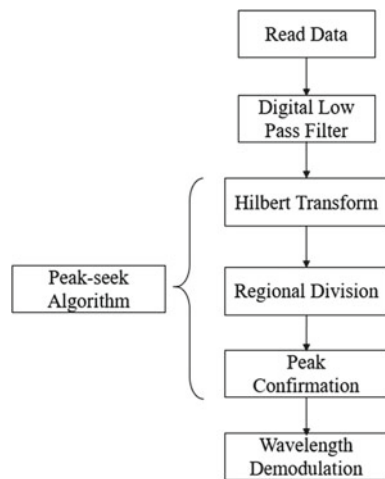
Fig. 2 FBG demodulation algorithm flow

Table 1 Performance comparison of FIR and IIR filters

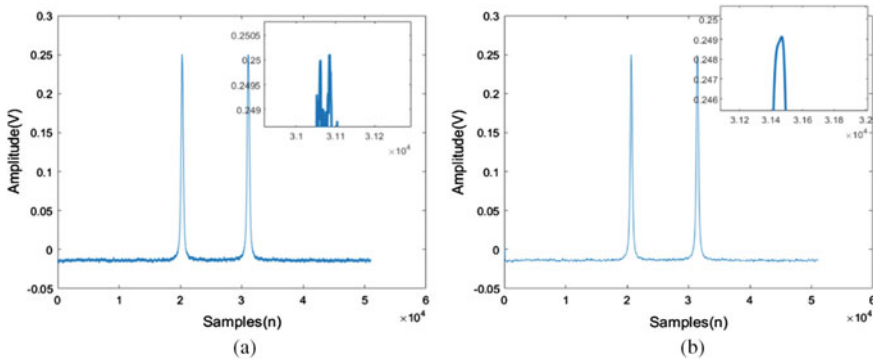|	Characteristic	Applications
FIR	Good linearity, strong stability, but computational complexity	System of image signal processing and other waveforms carrying information
IIR	Simple design, but pole offset can cause stability problems	Systems with low phase requirements such as voice communications

Fig. 3 **a** FBG reflectance spectrum raw data. **b** FBG digital filtered output

the loss of information as much as possible, FIR digital filters are used to process the data.

The raw data are the FBG reflection spectrum and the F-P etalon transmission spectrum, where all the sampling points in one scan period of the drive circuit are selected as the raw data. The time-domain waveform of the FBG raw data is shown in Fig. 3a.

The two peak signals in Fig. 3a correspond to the two FBG reflection spectra of the up and down travel of the tuned F-P filter driving voltage delta wave, respectively, and are evident from local amplification at the upper right corner, with some high-frequency noise in the original signal. Using the digital filter module in the Matlab toolbox, a low-pass filter with a cutoff frequency of 1 kHz was designed using a Hamming window, and the results are shown in Fig. 3b, where it can be found that the higher order harmonics near the FBG peak are filtered out, which will aid in the next step of the peak-seek algorithm processing. The same treatment was applied to the F-P etalon transmission spectrum, and the results are shown in Fig. 4.

3.2 Peak-Seek Algorithm Design

The peak-seek algorithm is to confirm that the optical signals of the F-P etalon and FBG are scanned by a tunable F-P filter, and the peak position of the electrical signal
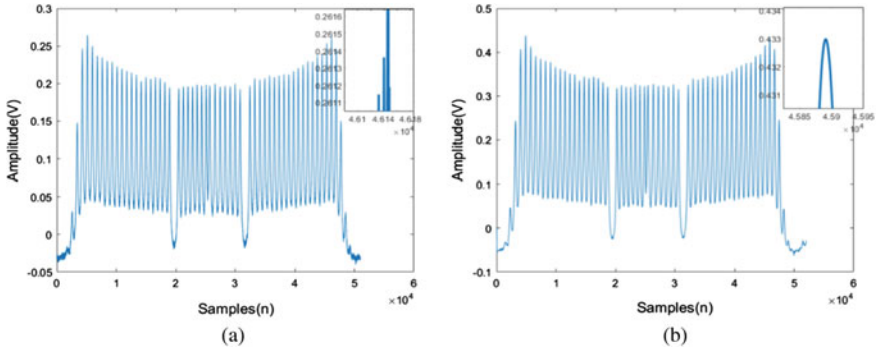
Fig. 4 **a** F-P etalon transmission spectrum raw data. **b** F-P etalon digital filtered output

after the optoelectronic conversion, with the peak value of each electrical signal corresponding to the central wavelength value of the optical signal. There are four commonly used peak-seek algorithms: direct peak-seek algorithm, power weighted peak-seek algorithm, general polynomial fitting, and Gaussian fitting algorithm.

The characteristics of various commonly used algorithms are shown in Table 2.

From the table, it can be seen that the Gaussian fitting algorithm has high peak finding accuracy and strong anti noise performance, so there are also the most improved algorithms based on the Gaussian algorithm (such as the Gaussian polynomial fitting algorithm). In order to reduce the calculation amount of the Gaussian fitting algorithm and adapt to the characteristic that the transmission spectrum of the F-P etalon contains multiple peak signals, this paper combines the Hilbert transform with the Gaussian fitting algorithm to complete the determination of the peak signal.

Table 2 Comparison of common peak-seek algorithms

	Accuracy	Noise immunity	Characteristic
Direct peak-seek algorithm	Low	Low	High sampling rate requirement
Power weighted peak-seek algorithm	Low	Low	High peak finding accuracy under low noise conditions
General polynomial fitting	Middle	Low	If the peak value is not within the sampling point, the error will be significant
Gaussian fitting algorithm	High	High	High accuracy and strong noise resistance, but complex calculations
Gaussian polynomial fitting algorithm	Middle	Low	Similar to general polynomial fitting methods, but with better accuracy and noise resistance

(1)   Hilbert transform

The function of Hilbert transform is to realize the predetermined bit and region segmentation of the peak value of the signal after low-pass filtering denoising, which can not only reduce the data volume of Gaussian fitting algorithm, but also eliminate the interference of other components in the signal to the fitting. Hilbert transform of time domain signal x(t) can be expressed as:

$$\hat{x}(t) = H[x(t)] = \frac{1}{\pi} \int_{-\infty}^{+\infty} x(\tau) \frac{1}{t - \tau} d\tau \tag{1}$$

where x(t) and $\hat{x}(t)$ are linear, and Hilbert transform can be expressed in convolution form:

$$\hat{x}(t) = H[x(t)] = x(t) * \frac{1}{\pi t} \tag{2}$$

Thus, the complexity of calculation $\hat{x}(t)$ is reduced. As shown in Fig. 5, Hilbert transform is performed on the filtered FBG reflection spectrum and F-P etalon transmission spectrum.

The signal peak after low-pass filtering is located between the two poles after Hilbert transform, so the sampling point interval corresponding to the two adjacent positive and negative poles can be used as the initial estimation of the peak position and peak interval. Compared with the constant threshold partition, Hilbert transform can overcome the problem of false peak detection caused by side lobe or peak distortion.

(2)   Gaussian fitting algorithm

Assuming the sampling data is $(x_i, y_i)(i = 1, 2, \ldots)$, the Gaussian fitting algorithm can be represented by Eq. (3):
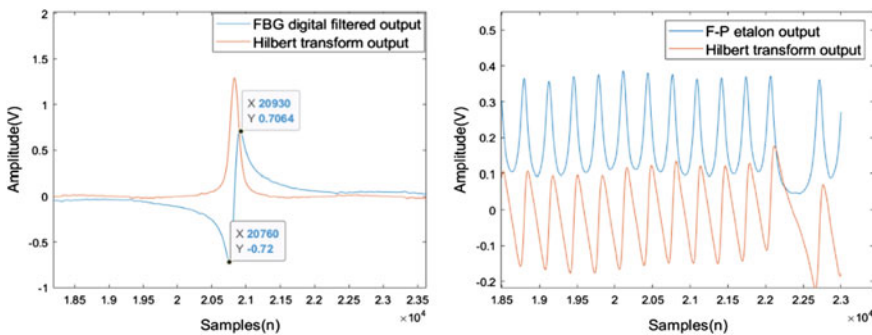

Fig. 5   Hilbert transform of FBG data and F-P etalon data

$$y_i = y_{max} \times \exp\left[f\left(\frac{x_i - x_{max}}{\sigma}\right)^2\right]f \tag{3}$$

In the formula, y_{max}, x_{max}, and σ are the peak values of the sampled data, the sampling points corresponding to the peak values, and the 3 dB bandwidth. For

$$z_i = \mathrm{In} y_i, \quad b_0 = \mathrm{In} y_{max} - \frac{x_{max}^2}{\sigma^2}, \quad b_1 = \frac{2x_{max}}{\sigma^2}, \quad b_2 = -\frac{1}{\sigma^2}$$

then Eq. (3) can be simplified as:

$$z_i = b_0 + b_1 x_i + b_2 x_i^2 \tag{4}$$

Substitute all data into Eq. (4), which can be expressed as $Z = XB$ by matrix, Expand to:

$$\begin{bmatrix} z_1 \\ z_2 \\ \vdots \\ z_n \end{bmatrix} = \begin{bmatrix} 1 & x_1 & x_1^2 \\ 1 & x_2 & x_2^2 \\ \vdots & \vdots & \vdots \\ 1 & x_n & x_n^2 \end{bmatrix} \begin{bmatrix} b_0 \\ b_1 \\ b_2 \end{bmatrix} \tag{5}$$

The least square solution of matrix B can be calculated by the least square principle

$$B = \left(X^T X\right)^{-1} X^T Z \tag{6}$$

Through the above analysis, the peak position can be expressed as:

$$x_{max} = -\frac{b_1}{2b_2} \tag{7}$$

Gaussian fitting curves can accurately calculate the center wavelength position. Due to its good mean square error, strong stability, and excellent noise resistance, it can effectively fit the spectral data of FBG and F-P etalon. The Gaussian fitting results are shown in Fig. 6.

3.3 Linear Interpolation Algorithm

Since the data acquisition module is used to simultaneously collect the signals of FBG and F-P etalon at the same sampling rate, the data of the two channels can be combined to solve the central wavelength value of FBG. The method is as follows: Confirm the sampling point corresponding to the center wavelength of each narrow-band spectrum through the negative peak marker point of the F-P etalon, and set the
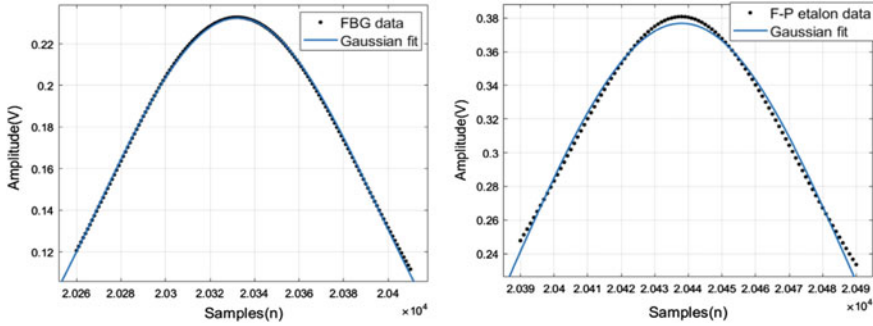
Fig. 6 Gaussian fitting of FBG data and F-P etalon data after threshold division

Table 3 Comparison of two peak-seek algorithms

Peak-seek algorithms	FBG1 error (pm)	FBG2 error (pm)
Gaussian fitting algorithm	5.14	5.08
Our peak-seek algorithm	0.56	0.63

center wavelengths of any two narrowband spectra of the F-P etalon as λ_1 and λ_2. The sampling points are x_1 and x_2 respectively, so the wavelength value corresponding to any sampling point λ_x can be obtained by Eq. (8)

$$\lambda_x = \frac{\lambda_2 - \lambda_1}{x_2 - x_1}(x - x_1) + \lambda_1 \tag{8}$$

The FBG center wavelength measured with a demodulator (SmartScan 08-80 XR, repeatability less than 1 pm) is the agreed true value, the comparison between the Gaussian fitting algorithm and the peak-seek algorithm designed in this article is shown in Table 3.

4 Conclusion

In this paper, firstly, digital low-pass filtering is performed on the collected original signal to remove high-frequency noise, and then Hilbert transform is introduced into the Gaussian fitting algorithm to solve the defect that the constant threshold division needs to predict the range of each peak, reducing the calculation amount of the Gaussian fitting algorithm. Finally, combined with the F-P etalon spectrum, the central wavelength of the FBG is extracted through the linear interpolation algorithm. The experiment shows that the peak finding error of the demodulation algorithm designed in this article is below 1 pm, which has certain reference value for engineering needs, especially for multi peak detection in distributed sensor networks.

References

1. Chen J, Liu B, Zhang H (2011) Review of fiber Bragg grating sensor technology. Front Optoelectron China 4:204–212
2. Shiratsuchi T, Imai T (2021) Development of fiber Bragg grating strain sensor with temperature compensation for measurement of cryogenic structures. Cryogenics 113:103233
3. Rosolem JB, Penze RS, Floridia C et al (2020) Dynamic effects of temperature on FBG pressure sensors used in combustion engines. IEEE Sens J 21(3):3020–3027
4. Duan Z, Jiang Y, Tai H (2021) Recent advances in humidity sensors for human body related humidity detection. J Mater Chem C 9(42):14963–14980
5. Li T, Guo J, Tan Y et al (2020) Recent advances and tendency in fiber Bragg grating-based vibration sensor: a review. IEEE Sens J 20(20):12074–12087
6. Song L, Fang F, Zhao J (2012) Study on viscosity measurement using fiber Bragg grating micro-vibration. Meas Sci Technol 24(1):015301
7. Hu Z, Pang C, Cheng F (2017) Application of Gaussian-LM algorithm in fiber Bragg grating reflection spectrum peak search. Laser Optoelectron Prog 54(1):013001
8. Jiang H, Guo Y, Zheng X et al (2020) Research on an improved spectral peak seeking algorithm with high precision. Study Opt Commun 46(1):33
9. Zhai X, Li Z (2020) Application of wavelet transform-based Gauss curve fitting in peak positioning. Opt Commun Technol 44(2):10–13
10. Djurhuus MSE, Werzinger S, Schmauss B et al (2019) Machine learning assisted fiber Bragg grating-based temperature sensing. IEEE Photon Technol Lett 31(12):939–942